Numerical modeling of fluid flow and time-lapse seismics to monitor CO_2 Sequestration in aquifers

J. E. Santos[1]

[1] CONICET, IGPUBA, Fac. Ing., UBA and Univ. Nac. de La Plata, ARGENTINA ,
and Department of Mathematics, Purdue University

Work with G. B. Savioli (IGPUBA), J. M. Carcione and D. Gei ((OGS), Trieste, ITALY).

IMAL, 30/5/2014

Introduction. I

- Storage of CO_2 in geological formations is a procedure employed to reduce the amount of greenhouse gases in the atmosphere to slow down global warming.
- Geologic sequestration involves injecting CO_2 into a target geologic formation at depths typically $>$ 1000 m where pressure and temperature are above the critical point for CO_2 (31.6C, 7.38 MPa).
- First industrial scale CO_2 injection project: Sleipner gas field (North Sea).

Introduction. II

- CO_2 is separated from natural gas produced and is currently being injected into the Utsira Sand, a saline aquifer at the Sleipner field, some 26000 km^2 in area.
- Injection started in 1996 at a rate of about one million tonnes per year.
- Time-lapse seismic surveys aim to monitor the migration and dispersal of the CO_2 plume after injection.
- Very little is known about the effectiveness of CO_2 sequestration over very long periods of time.

Introduction. III

- The analysis of CO_2 underground storage safety in the long term is a current area of research.
- We present a methodology integrating numerical simulation of CO_2-brine flow and seismic wave propagation to model and monitor CO_2 injection.
- The model of the formation is based on the porosity and clay content distribution considering the variation of properties with fluid pressure and saturation.
- The model considers the geometrical features of the formations, including the presence of shale seals and fractures and fractal variations of the petrophysical properties.

Presentation Outline

- Present the two-phase fluid flow equations used to simulate CO_2 injection.
- Describe a viscoelastic model for wave propagation
- Present a petrophysical model of a shaly sandstone based on fractal porosity and clay content, considering the variation of properties with pressure and saturation.
- Show numerical simulations of CO_2 injection and time-lapse seismics to monitor the migration and dispersal of CO_2 after injection in the Utsira formation at the Sleipner field in the North Sea.

The Black-Oil formulation

- The simultaneous flow of brine and CO_2 is described by the well-known **Black-Oil formulation** applied to two-phase, two component fluid flow.
- In the **Black-Oil** model employed, brine is NOT present, OIL is identified with brine and CO_2 is identified with GAS.
- Also, CO_2 may dissolve in brine (OIL) but brine (OIL) is not allowed to vaporize into the CO_2 phase.
- This formulation uses, as a simplified thermodynamic model, the quantities R_s, B_b and B_{CO2} as PVT data:

The Black-Oil formulation of two-phase flow in porous media. I

- $R_s = \frac{V_{dCO2}^{SC}}{V_b^{SC}}$: **$CO_2$ solubility in brine**
- $B_{CO2} = \frac{V_{CO2}^{res}}{V_{CO2}^{SC}}$: **$CO_2$ formation volume factor**
- $B_b = \frac{(V_{dCO2}^{res} + V_b^{res})}{V_b^{SC}}$: **brine formation volume factor**

To estimate the above PVT data we used an algorithm developed by Hassanzadeh (2008).

The Black-Oil equations for two-phase flow in porous media are obtained combining conservation of mass of each component with two-phase Darcy's law.

The Black-Oil formulation of two-phase flow in porous media. II

$$\nabla \cdot \left[\frac{\underline{\kappa} k_{rCO2}}{B_{CO2}\eta_{CO2}} (\nabla p_{CO2} - \rho_{CO2} g \nabla D) + \frac{\underline{\kappa} R_s k_{rb}}{B_b \eta_b} (\nabla p_b - \rho_b g \nabla D) \right]$$

$$+ q_{CO2} = \frac{\partial \left[\phi \left(\frac{S_{CO2}}{B_{CO2}} + \frac{R_s S_b}{B_b} \right) \right]}{\partial t}$$

$$\nabla \cdot \left[\frac{\underline{\kappa} k_{rb}}{B_b \eta_b} (\nabla p_b - \rho_b g \nabla D \right] + q_b = \frac{\partial \left[\phi \frac{S_b}{B_b} \right]}{\partial t}$$

Two algebraic equations complete the system:

$$S_b + S_{CO2} = 1, \qquad p_{CO2} - p_b = P_C(S_b)$$

Numerical solution of the Black-Oil formulation of two-phase flow in por

The unknowns for the Black-Oil fluid-flow model are the fluid pressures p_{CO2}, p_b and the saturations S_{CO2}, S_b for the CO_2 and brine phases.

They were computed using the public domain software BOAST, which solves the differential equations applying IMPES, a finite difference technique.

Seismic modeling. Mesoscopic attenuation effects. I

- An important mechanism of P-wave attenuation and dispersion at seismic frequencies is known as mesoscopic loss, due to heterogeneities larger than the pore size but much smaller than the predominant wavelengths (mesoscopic-scale heterogeneities).
- These effects are due to the equilibration of wave-induced fluid pressure gradients via a slow-wave diffusion process (Type II Biot waves).
- White et al. (1975) were the first to introduce the mesoscopic-loss mechanism in the framework of Biot's theory, which is illustrated in the next figures.

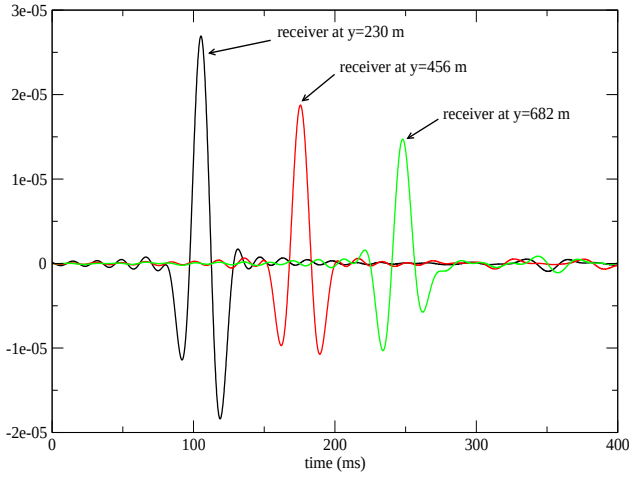

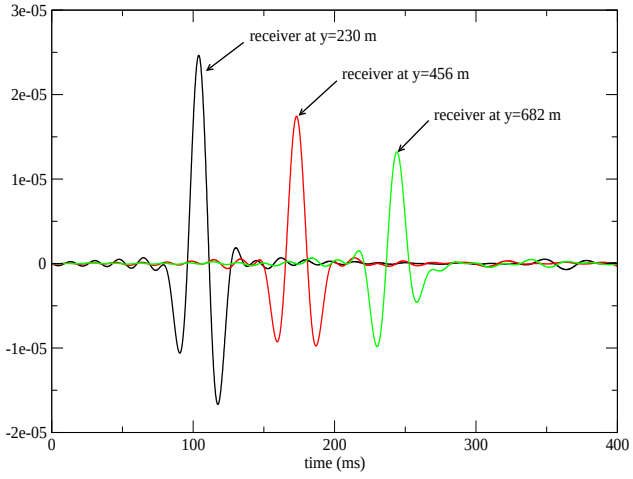

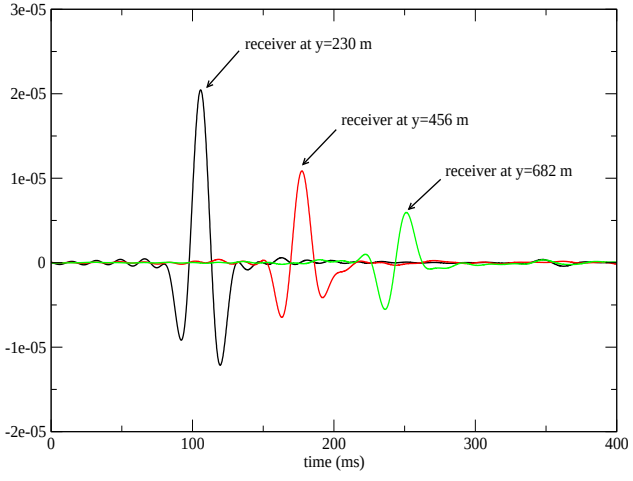

Waves travelling in porous media saturated by gas (top left), water (top right) and periodic gas-water (bottom

Waves travelling in a porous media with gas, water and periodic gas-water saturation

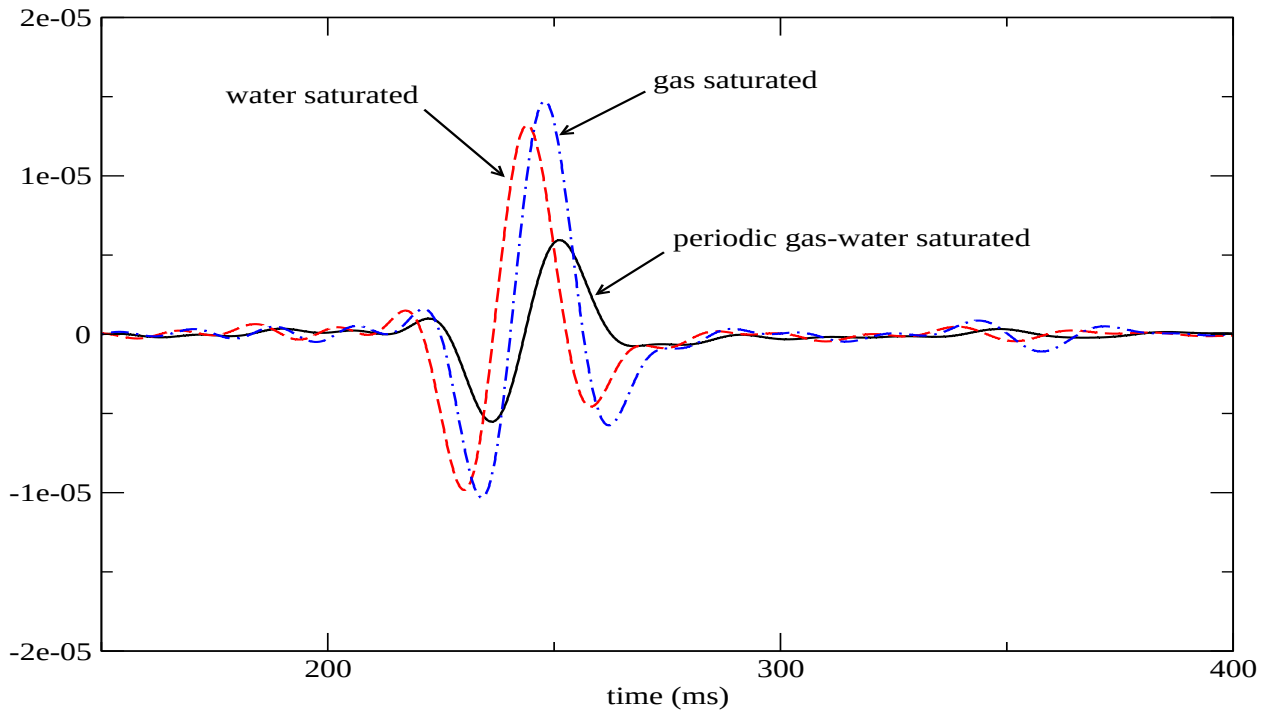

The delay in the arrival time in the periodic case is due to the velocity dispersion caused by the mesoscopic scale heterogeneities. Attenuation and dispersion in the periodic gas-water case is in perfect agreement with that predicted by White's theory.

Patchy CO_2-brine saturation and associated normalized fluid pressure. Frequency is 50 Hz.

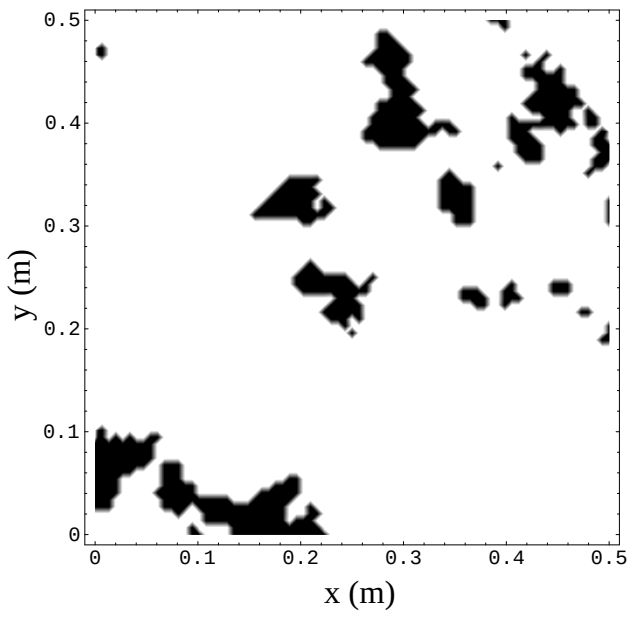

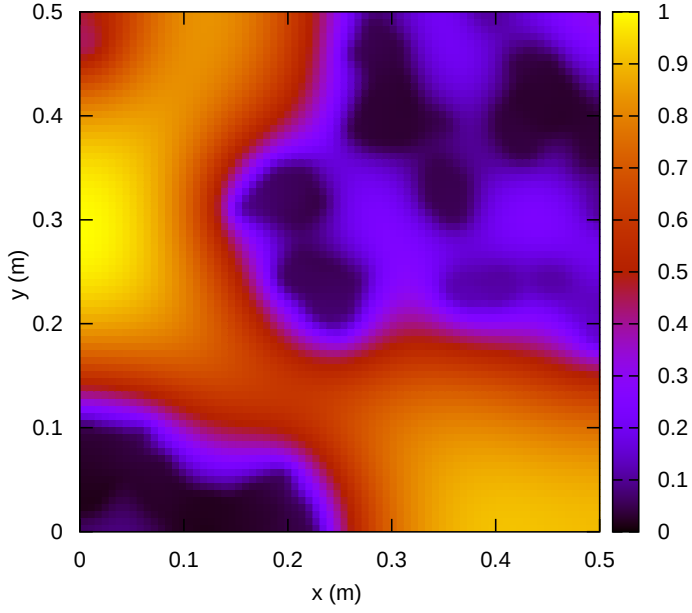

Patchy CO_2-brine saturation (left, black zones correspond to pure CO_2 saturation) and normalized fluid-pressure amplitude distribution (right). The domain is a square of side length 50 cm. Overall CO_2 saturation is 10 %. Attenuation and velocity dispersion (mesoscopic loss) is caused by fluid flow between regions of different pore pressures

Computed Vp (P-wave phase velocity) as function of CO_2 patchy saturation

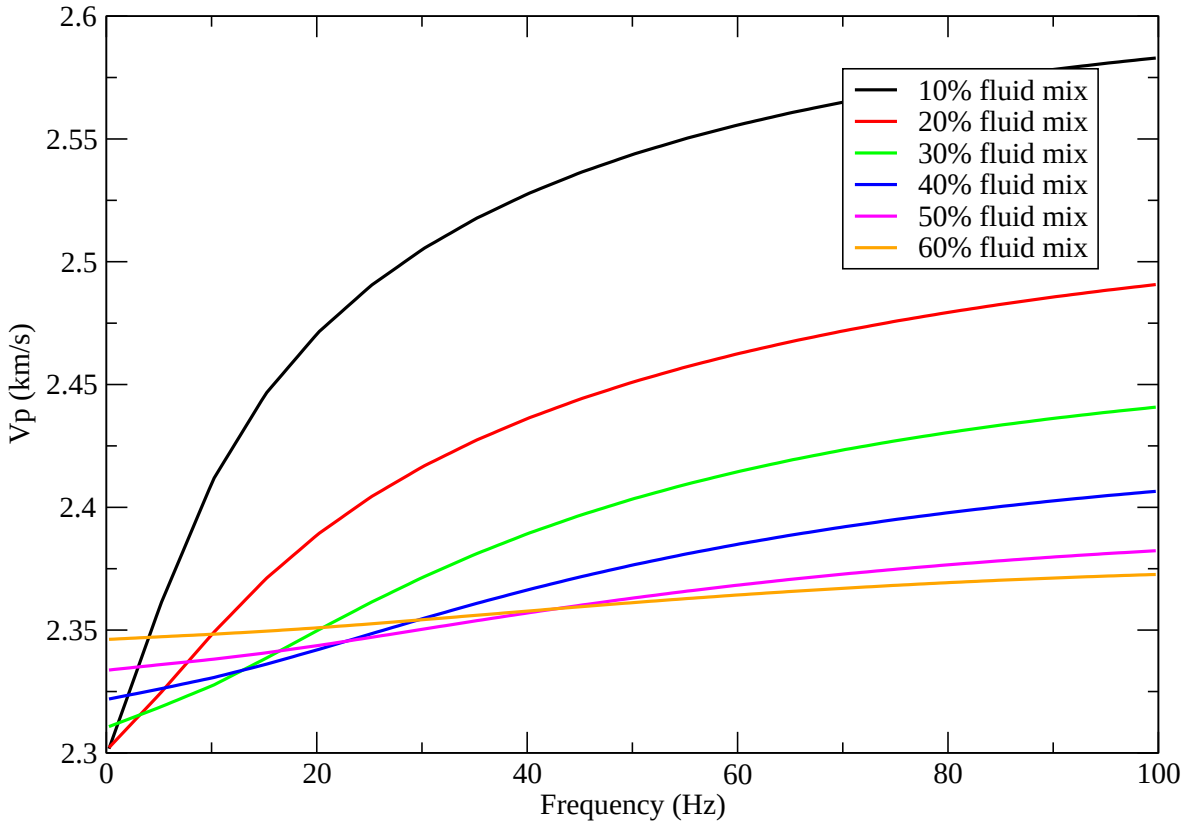

CO_2 is in gaseous state, fractal dimension D=2.5, correlation length a = 5 cm

Computed inverse quality factor as function of CO_2 patchy saturation

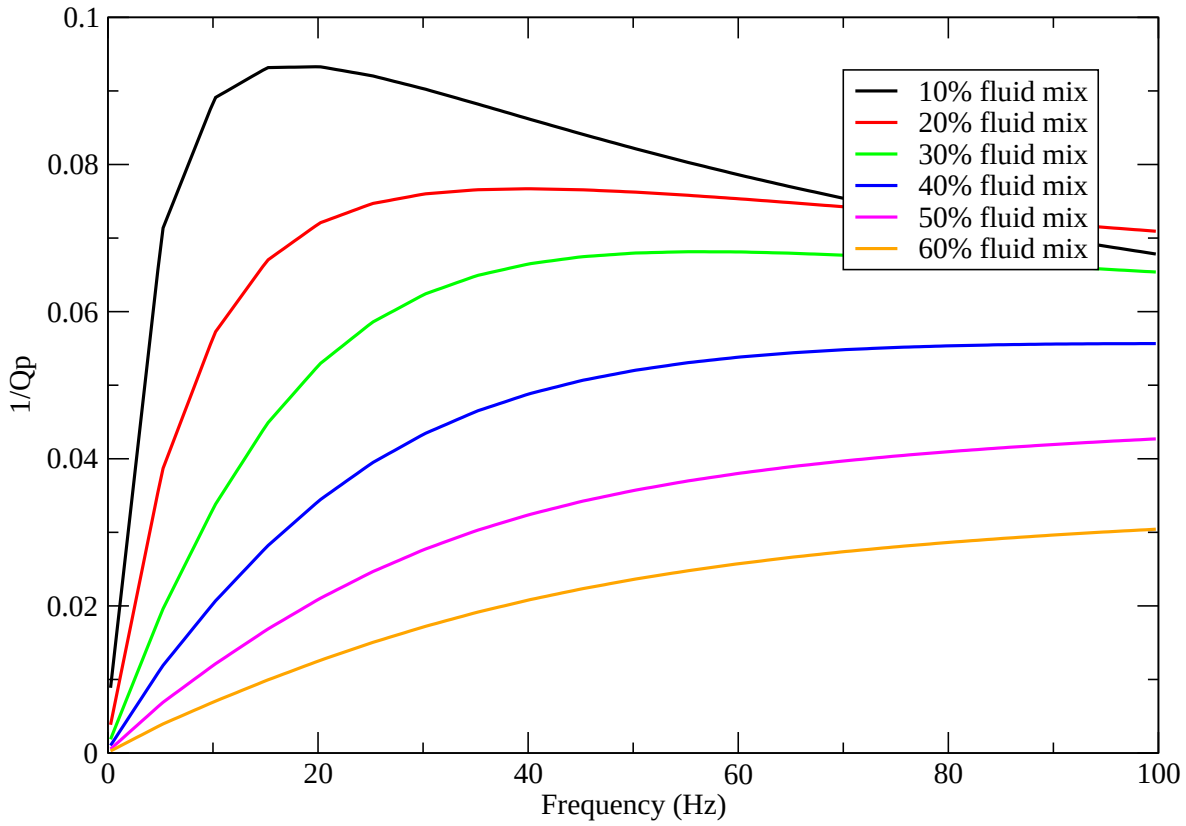

CO_2 is in gaseous state, fractal dimension D=2.5, correlation length a = 5 cm

Computed Vp and 1/Qp as function of CO_2 patchy saturation.

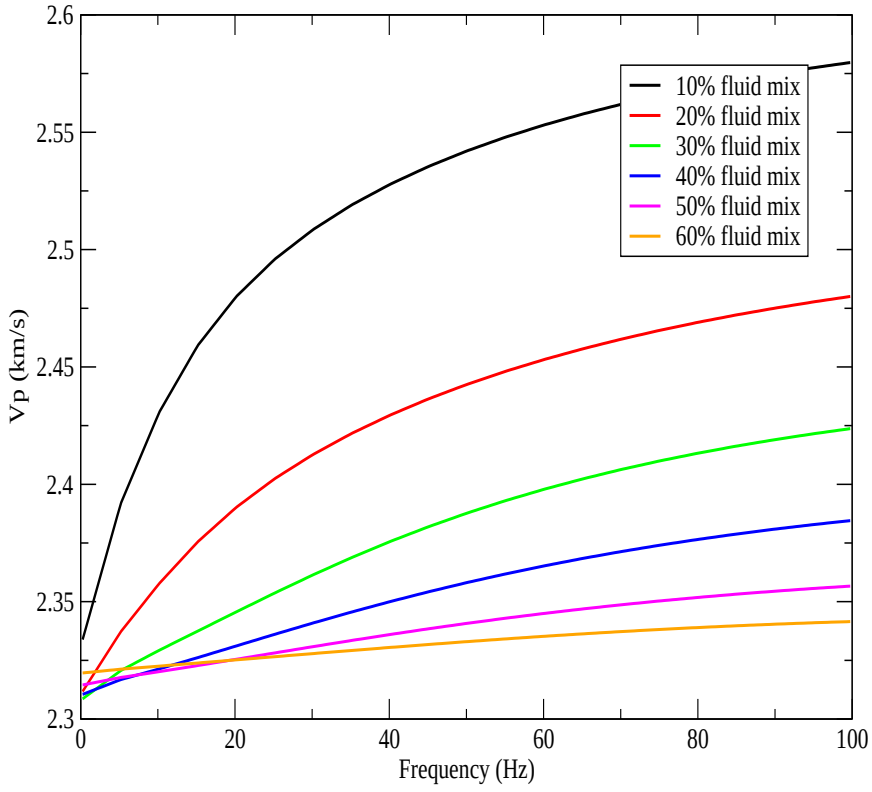

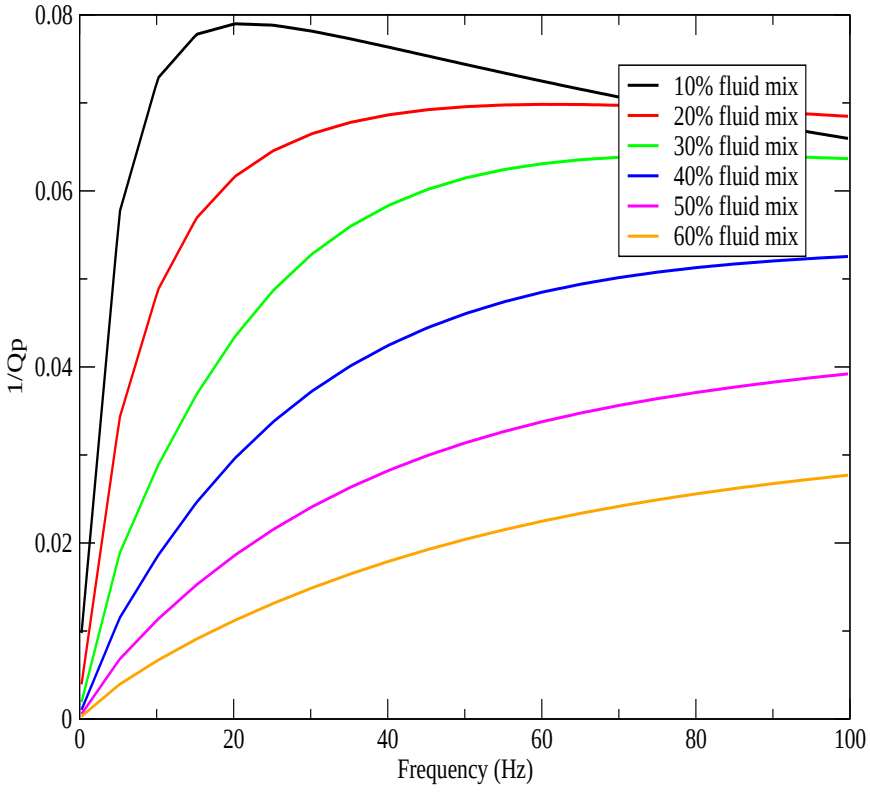

CO_2 is in liquid state, fractal dimension D=2.5, correlation length a = 5 cm

Computed Vp and 1/Qp as function of CO_2 patchy saturation.

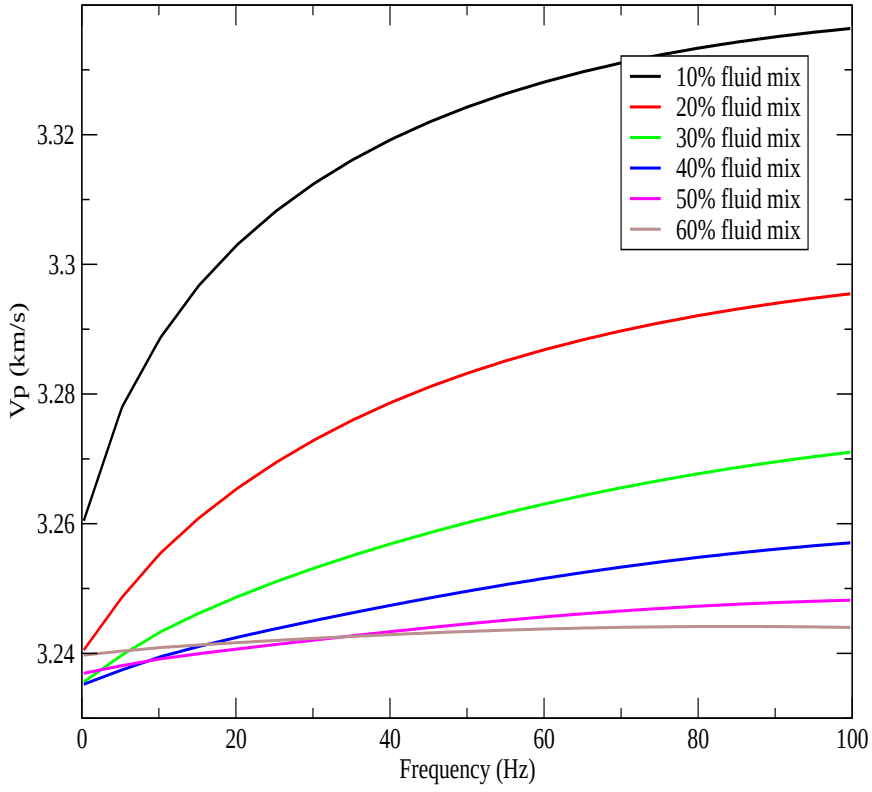

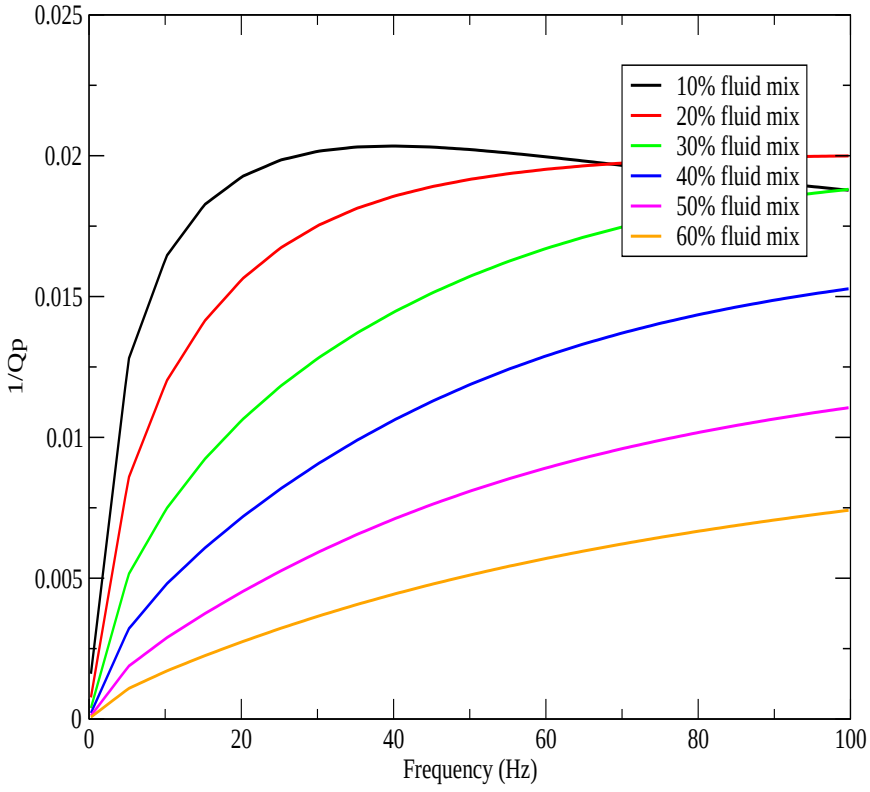

CO_2 is in supercritical state, fractal dimension D=2.5, correlation length a = 5 cm

Seismic modeling. Mesoscopic attenuation effects. II

- Due to the **extremely fine meshes** needed to properly represent these type of media, numerical simulations at the macroscale is very expensive or even not feasible.
- Our approach: employ an **upscaling procedure** to include at the macroscale the mesoscale effects.
- At the bottom and top of the Utsira formation and in the mudstone layers inside the Utsira formation the **complex bulk and shear moduli** as function of frequency were determined using a Zener model.

Seismic modeling. Mesoscopic attenuation effects. III

- Within the Utsira formation and outside the mudstone layers, we determine complex and frequency dependent P-wave modulus

$$E(\omega) = \lambda(\omega) + 2\mu(\omega)$$

  at the mesoscale using White's theory for patchy saturation.
- $\lambda(\omega), \mu(\omega)$: Lamé coefficients
- ω : angular frequency

Seismic modeling. Mesoscopic attenuation effects. IV

- Shear wave attenuation is taken into account using another relaxation mechanism related to the P-wave White mechanism to make the shear modulus

$$\mu(\omega)$$

  complex and frequency dependent.

- These complex moduli define an equivalent viscoelastic model at the macroscale that takes into account dispersion and attenuation effects occurring at the mesoscale.

Seismic modeling. Constitutive Relations

$u = u(\omega) = (u_x(\omega), u_z(\omega))$: **Time-Fourier transform of the displacement vector**

Stress-strain relations in the space-frequency domain:

$$\sigma_{jk}(u) = \lambda(\omega)\nabla \cdot u\delta_{jk} + 2\mu(\omega)\varepsilon_{jk}(u),$$

$\sigma_{jk}(u)$: **stress tensor** $\varepsilon_{jk}(u)$: **strain tensor**

δ_{jk}: **Kroenecker delta**

Seismic modeling. Phase velocities and attenuation coefficient.

For isotropic viscoelastic solids, the frequency dependent phase velocities $v_t(\omega)$ and quality factors $Q_t(\omega)$, $t = p, s$ are defined by the relations

$$v_t(\omega) = \left[\mathrm{Re}\left(\frac{1}{vc_t(\omega)}\right)\right]^{-1}, \; Q_t(\omega) = \frac{\mathbf{Re}(vc_t(\omega)^2)}{\mathbf{Im}(vc_t(\omega)^2)}, \; t = p, s$$

$vc_p(\omega), vc_s$**: complex and frequency dependent compressional and shear velocities defined as**

$$vc_p(\omega) = \sqrt{\frac{E(\omega)}{\rho}}, \quad vc_s(\omega) = \sqrt{\frac{\mu(\omega)}{\rho}}$$

ρ**: bulk density.**

Seismic modeling. A viscoelastic model for wave propagation.

Equation of motion in a 2D isotropic viscoelastic domain Ω with boundary $\partial\Omega$:

$$\omega^2 \rho u + \nabla \cdot \sigma(u) = f(x,\omega), \quad \Omega$$
$$-\sigma(u)\nu = i\omega \mathcal{D} u, \quad \partial\Omega,$$

$f(x,\omega)$ **external source**

$$\mathcal{D} = \rho \begin{bmatrix} \nu_1 & \nu_2 \\ -\nu_2 & \nu_1 \end{bmatrix} \begin{bmatrix} v_p(\omega) & 0 \\ 0 & v_s(\omega) \end{bmatrix} \begin{bmatrix} \nu_1 & -\nu_2 \\ \nu_2 & \nu_1 \end{bmatrix},$$

$\nu = (\nu_1, \nu_2)$**: the unit outward normal on** $\partial\Omega$

Numerical Solution - Finite Element Method.

- The FE space-frequency solution of the viscoelastic wave equation was computed at a selected number of frequencies in the range of interest using an **iterative FE domain decomposition procedure**.
- To approximate each component of the solid displacement vector we employed a **nonconforming FE space** NC^h defined over a partition of the domain Ω into rectangles of diameter bonded by h.
- The use of the FE space NC^h generates **less numerical dispersion than the standard bilinear elements**. The error of the FE procedure is of order $h^{1/2}$
- The time domain solution was obtained using a discrete inverse Fourier transform.

Numerical Solution - Finite Element Method.

Lagrange multipliers λ_{jk}^h: associated with the stress values $-\sigma(u_j)\nu_{jk}(\xi_{jk})$:

$$\widetilde{\Lambda}^h = \{\lambda^h \colon \lambda^h|_{\Gamma_{jk}} = \lambda_{jk}^h \in [P_0(\Gamma_{jk})]^2 = [\Lambda_{jk}^h]^2\}.$$

$P_0(\Gamma_{jk})$ **are constant functions on** Γ_{jk}**. Note that** Λ_{jk}^h **and** Λ_{kj}^h **are considered to be distinct. A discrete domain decomposition (hybridized) iterative algorithm:**

Numerical Solution - Finite Element Method.

Given an initial guess $\left(\widehat{u}_j^{h,0}, \lambda_{jk}^{h,0}, \lambda_{kj}^{h,0}\right) \in [NC_j^h]^2 \times [\Lambda_{jk}^h]^2 \times [\Lambda_{kj}^h]^2$**,**

compute $\left(\widehat{u}_j^{h,n}, \lambda_{jk}^{h,n}\right) \in [NC_j^h]^2 \times [\Lambda_{jk}^h]^2$ **as the solution of the equations**

$$-(\rho\omega^2\widehat{u}_j^{h,n}, \varphi)_j + \sum_{pq}(\tau_{pq}(\widehat{u}^{h,n}), \varepsilon_{pq}(\varphi))_j + i\omega\left\langle\left\langle \mathcal{A}\widehat{u}_j^{h,n}, \varphi\right\rangle\right\rangle_{\Gamma_j}$$

$$+\sum_k \left\langle\left\langle \lambda_{jk}^{h,n}, \varphi\right\rangle\right\rangle_{\Gamma_{jk}} = (\widehat{f}, \varphi)_j, \quad \varphi \in [NC_j^h]^N,$$

$$\lambda_{jk}^{h,n} = -\lambda_{kj}^{h,n-1} + i\beta_{jk}[\widehat{u}_j^{h,n}(\xi_{jk}) - \widehat{u}_k^{h,n-1}(\xi_{jk})], \qquad \textbf{on } \Gamma_{jk}.$$

It can be shown that if u^h is the solution of the global FE procedure,

$$\|u^{h,n} - u^h\|_0 \to 0 \text{ in } [L^2(\Omega)]^2 \quad \text{when} \quad n \to \infty,$$

A petrophysical model for the Utsira formation. I

Pressure dependence of the petrophysical properties:

$$\frac{(1-\phi_c)}{K_s}(p(t)-p_H) = \phi_0 - \phi(t) + \phi_c \ln \frac{\phi(t)}{\phi_0}, \qquad (1)$$

$p(t) = S_b p_b(t) + S_g p_g(t)$ **: pore pressure,**

ϕ_c**: critical porosity**

ϕ_0**: initial porosity at hydrostatic pore pressure** $p_H = \rho_b g z$

(g **the gravity constant,** z **is depth (in km b.s.l.))**

ρ_b **= 1040 kg/m**^{3}**: brine density**

K_s**: bulk modulus of the solid grains**

A petrophysical model for the Utsira formation. II.

Relationship among horizontal permeability κ_x porosity ϕ and clay content C is

$$\frac{1}{\kappa_x(t)} = \frac{45(1-\phi(t))^2}{\phi(t)^3}\left(\frac{(1-C)^2}{R_q^2} + \frac{C^2}{R_c^2}\right)$$

R_q, R_c**: average radii of sand and clay particles As permeability is anisotropic, we assume the following relationship between horizontal and vertical permeability κ_z**

$$\frac{\kappa_x(t)}{\kappa_z(t)} = \frac{1-(1-0.3a)\sin(\pi S_b(t))}{a(1-0.5\sin(\pi S_b(t)))}$$

a**: permeability-anisotropy parameter**

A petrophysical model for the Utsira formation. III.

The bulk modulus of the dry matrix was determined using a Krief model ($A = 4.5$):

$$K_m = K_s(1-\phi)^{A/(1-\phi)}.$$

Assuming a Poisson medium the shear modulus of the solid grains is $\mu_s = 3K_s/5$ and the following relation gives the shear modulus of the dry matrix

$$\mu_m = \mu_s(1-\phi)^{A/(1-\phi)}.$$

A model for the Utsira formation. I

- The model of the Utsira formation has
  1.2 km in the x-direction,
  10 km in the y-direction
  0.4 km in the z-direction
  (top at 0.77 km and bottom at 1.17 km b.s.l.).
- Within the Utsira formation, there are several mudstone layers which act as barriers to the vertical motion of the CO_2.
- The initial porosity ϕ_0 is assumed to have a fractal spatial distribution based on the von Karman self-similar correlation functions. The corresponding permeabilities κ_x, κ_z were determined for a fixed clay content $C = 6\%$

A model for the Utsira formation. II

- The mudstone layers are not completely sealed, having constant porosity and vertical permeability values of 24 % and 0.033 D.
- The mudstone layers have openings, that will give a path for the upward migration of CO_2.
- The top and bottom of the Utsira formation have constant porosity and vertical permeability values of 22 % and 0.02 D.

Initial porosity ϕ_0 of the formation before CO_2 injection.

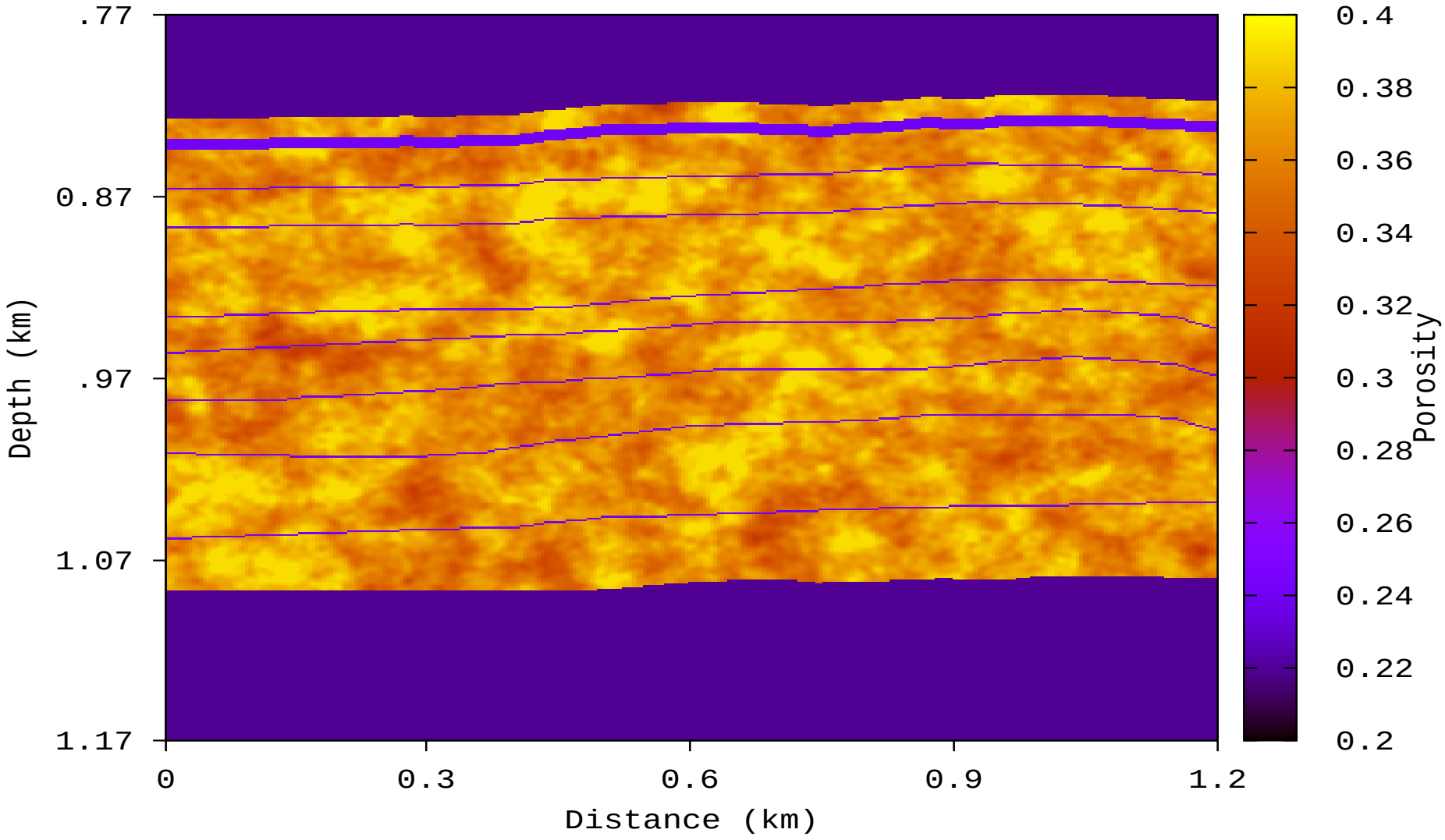

Fractal dimension is $D = 2.2$, average porosity is $\langle \phi_0 \rangle$ = 36.7 %. Correlation length is 2% of the domain size.

CO_2 Injection model. I

- At the Utsira formation CO_2 is injected at a constant flow rate of one million tons per year at $x = 0.6$ km, $z = 1.082$ km
- The flow simulation mesh: $n_x = 300$ in the x-direction, $n_y = 5$ in the y-direction and $n_z = 400$ in the z-direction.
- The model is 2.5D since the properties are uniform along the y-direction, which has an extension of 10 km.
- The source is located at the third grid point along the y-direction.

CO_2 Injection model. II

- The petrophysical properties of the formation are time dependent due to the CO_2 injection and the consequent increase in pore fluid pressure.
- These properties change at a much slower rate than pressure and saturation.
- Hence, we have two time scales, and we use a much larger time step to update petrophysical properties than to run the flow simulator.
- In this work, the petrophysical properties are updated every year, while the time step for the flow simulator is 0.125 d.

2D slices (at ny=3) of the vertical permeability κ_z distribution

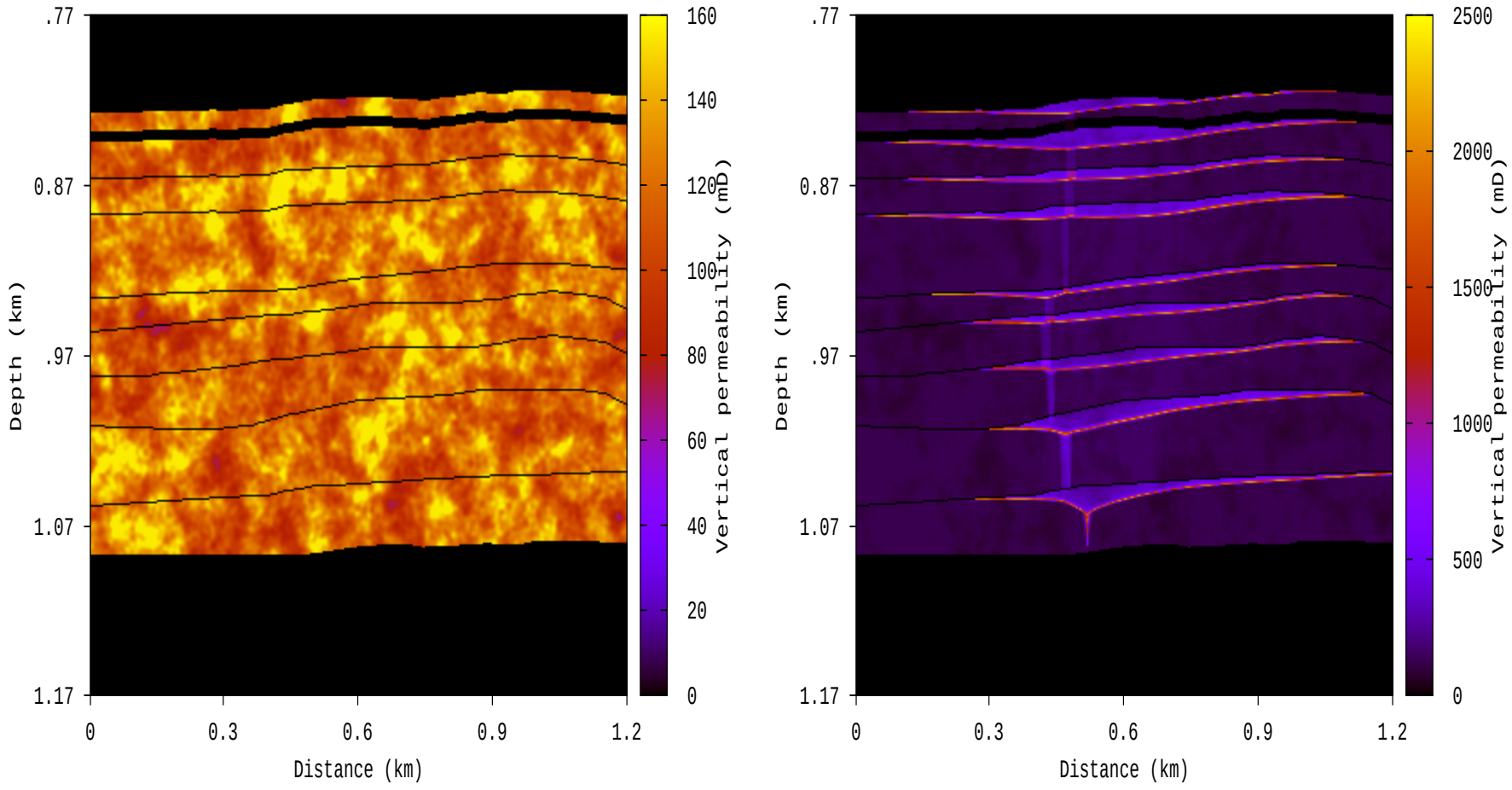

Initial vertical permeability distribution (left) and after seven years of CO_2 injection (right). Recall that κ_z is a function of CO_2 saturation.

2D slices (at $n_y = 3$) of the CO_2 saturation field.

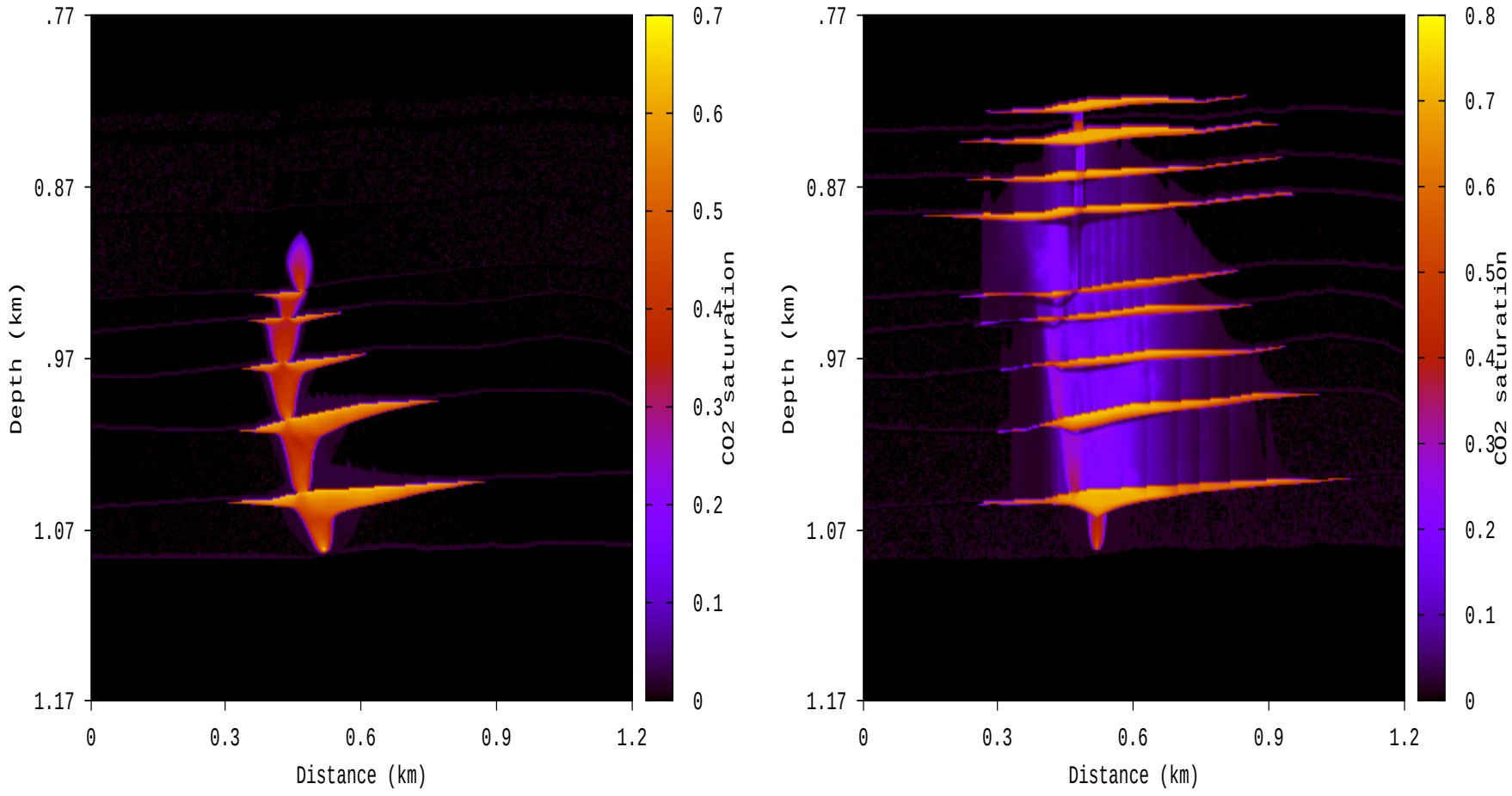

CO_2 saturation distribution after one year (left) and three years (right) of CO_2 injection. As injection proceeds, part of the injected fluid migrates upwards, generating chimneys.

2D slices (at $n_y = 3$) of the CO_2 saturation field.

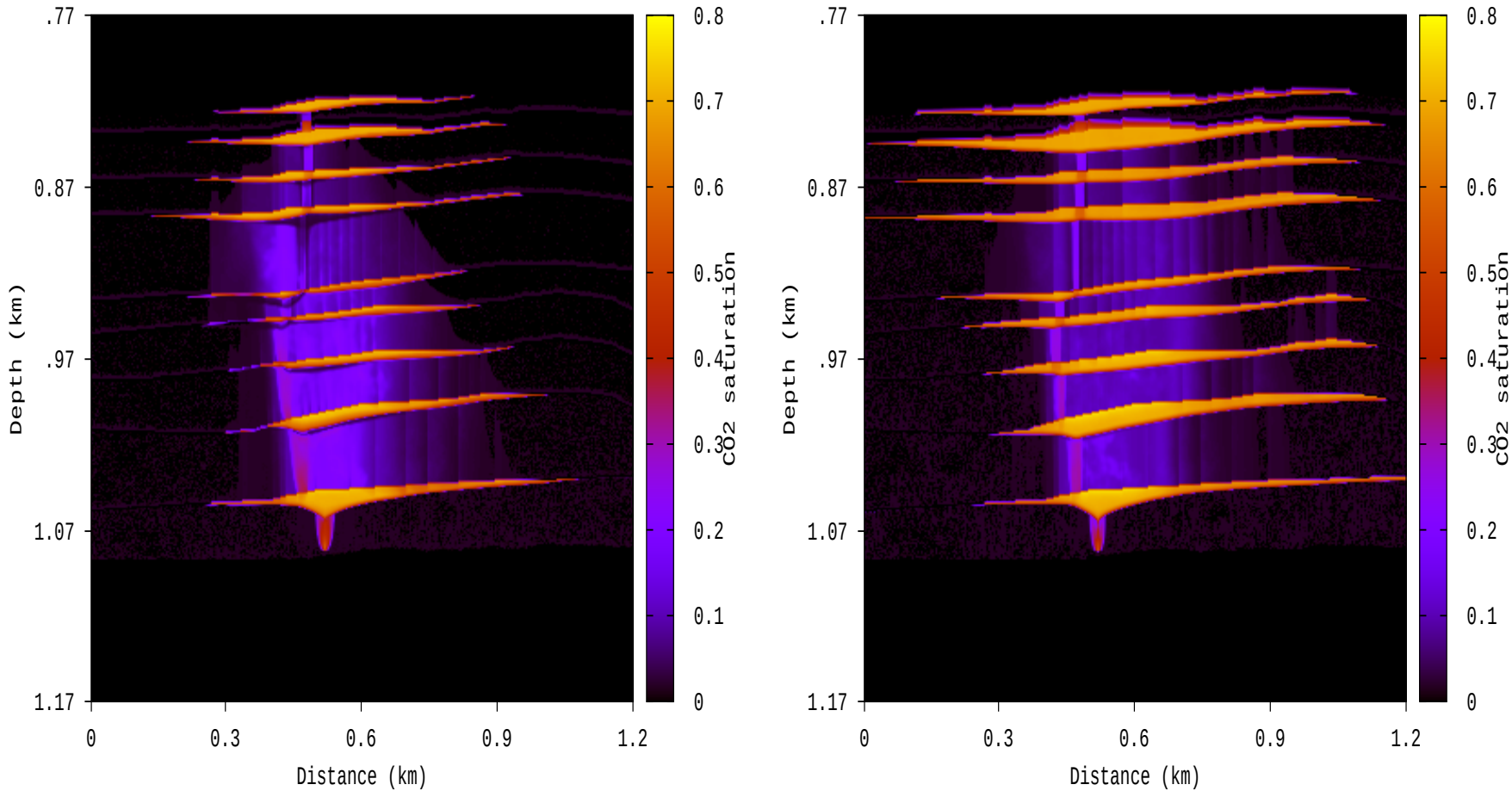

CO_2 saturation distribution after three years (left) and seven years (right) of CO_2 injection. As injection time increases, chimneys become less defined, with regions of low CO_2 saturations between layers.

Seismic Model.

- We use 2D slices (at $n_y = 3$) of CO_2 saturation and fluid pressure obtained from the flow simulator to build a 2D model of the Utsira formation.
- The time Fourier transforms of the displacement vector was computed for 200 temporal frequencies in $(0, 200\text{Hz})$.
- The seismic source was a spatially localized plane wave of main frequency 60 Hz at depth $z = 772$ m (top of the model).
- A line of receivers was located at the same depth to record the Fourier transforms of the vertical displacements.
- The next Figures show maps of the wave velocities and quality factors for the model.

P-wave phase velocity at 60 Hz before (left) and after seven years (right) of CO_2 injection

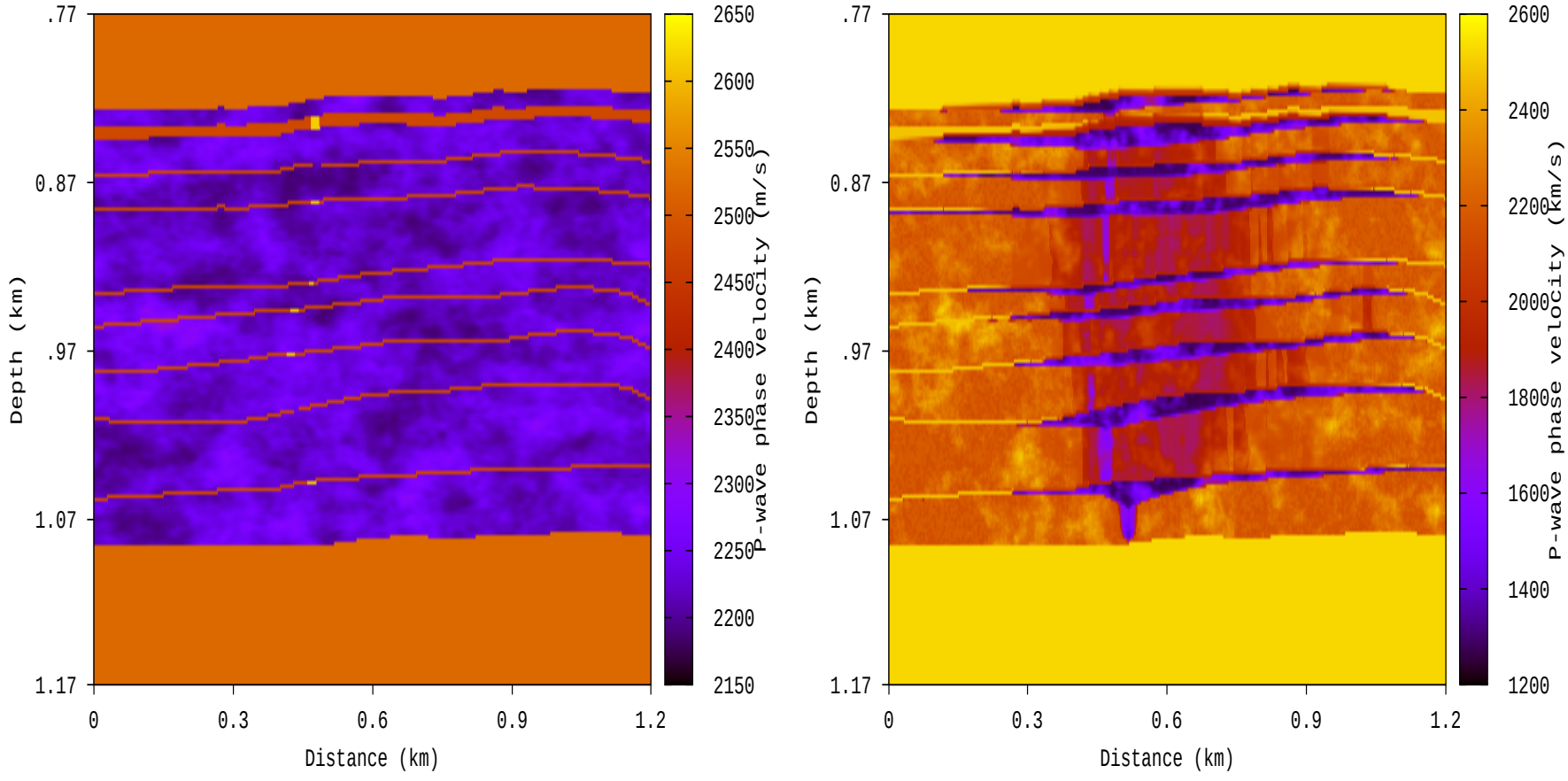

Note a decrease in P- wave velocity in zones of CO_2 accumulation.

S-wave phase velocity at 60 Hz before (left) and after seven years (right) of CO_2 injection

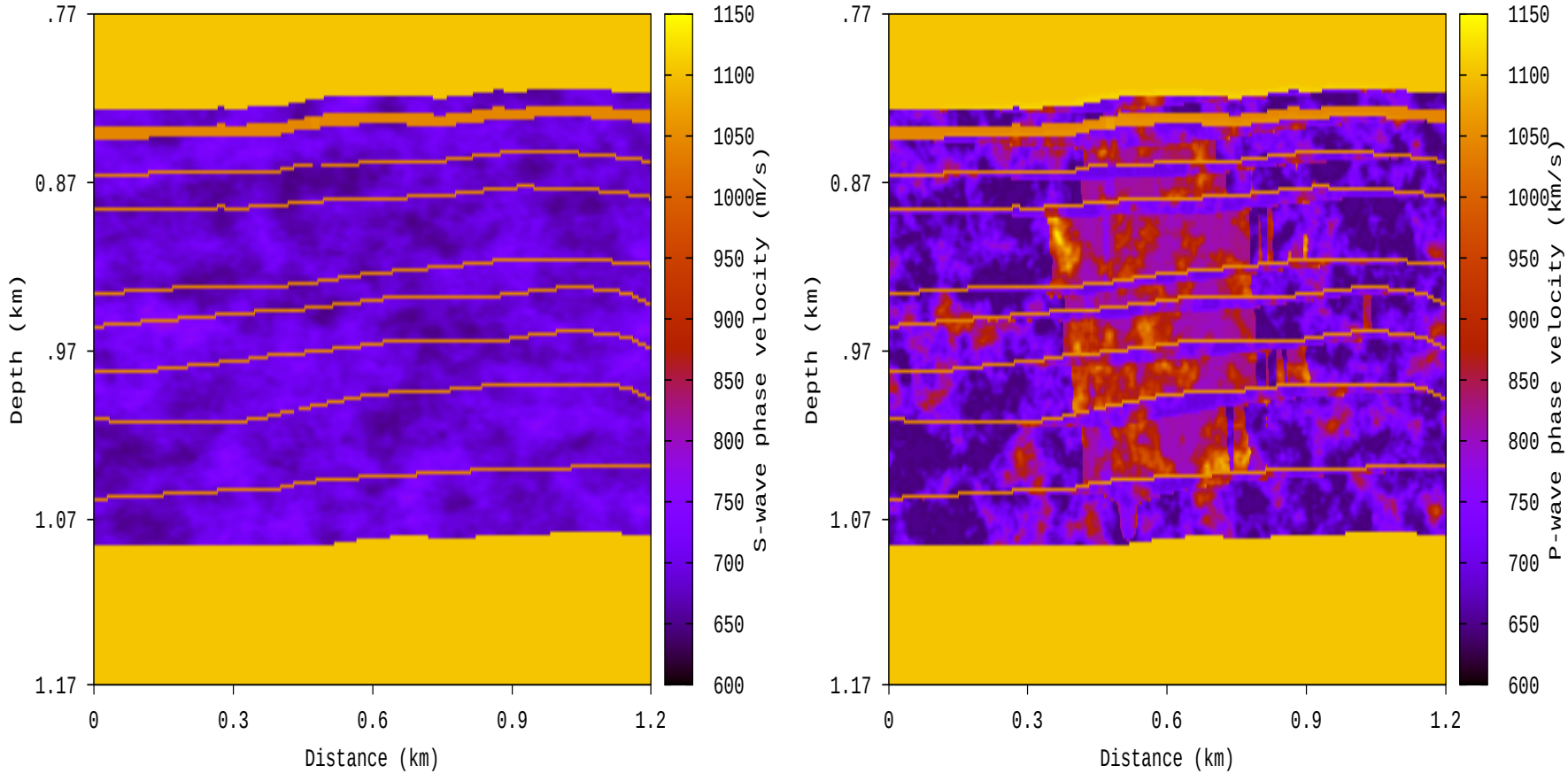

Note an increase in S- wave velocity in zones of CO_2 accumulation.

P-wave phase velocity (left) and quality factor (right) at 60 Hz after seven years of CO_2 injection.

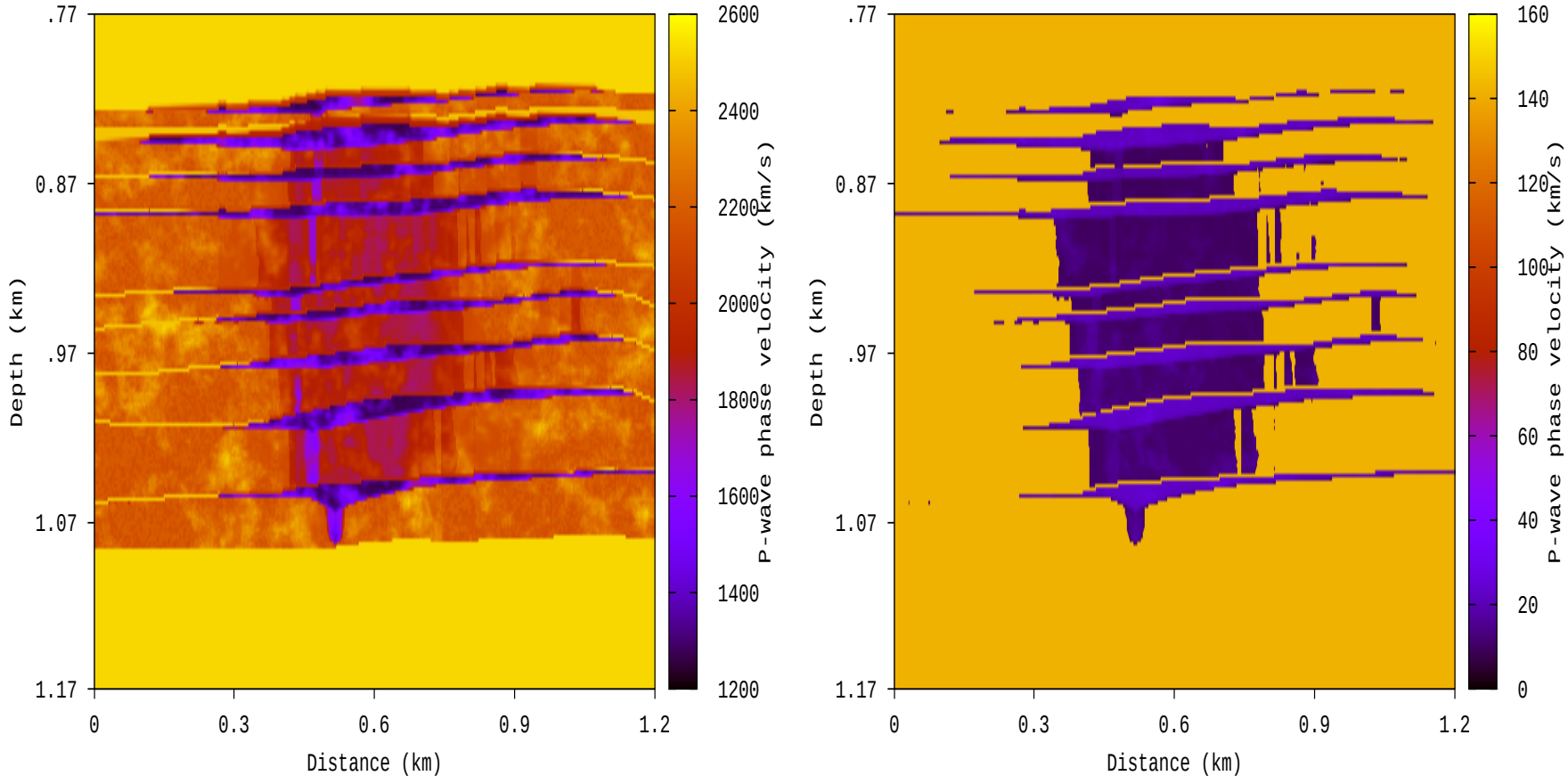

Note a decrease in P- wave velocity v_p in zones of CO_2 accumulation and a corresponding decrease in the quality factor Q_p indicating regions of higher P-wave attenuation.

Synthetic seismograms before (left) and after one year (right) of CO_2 injection.

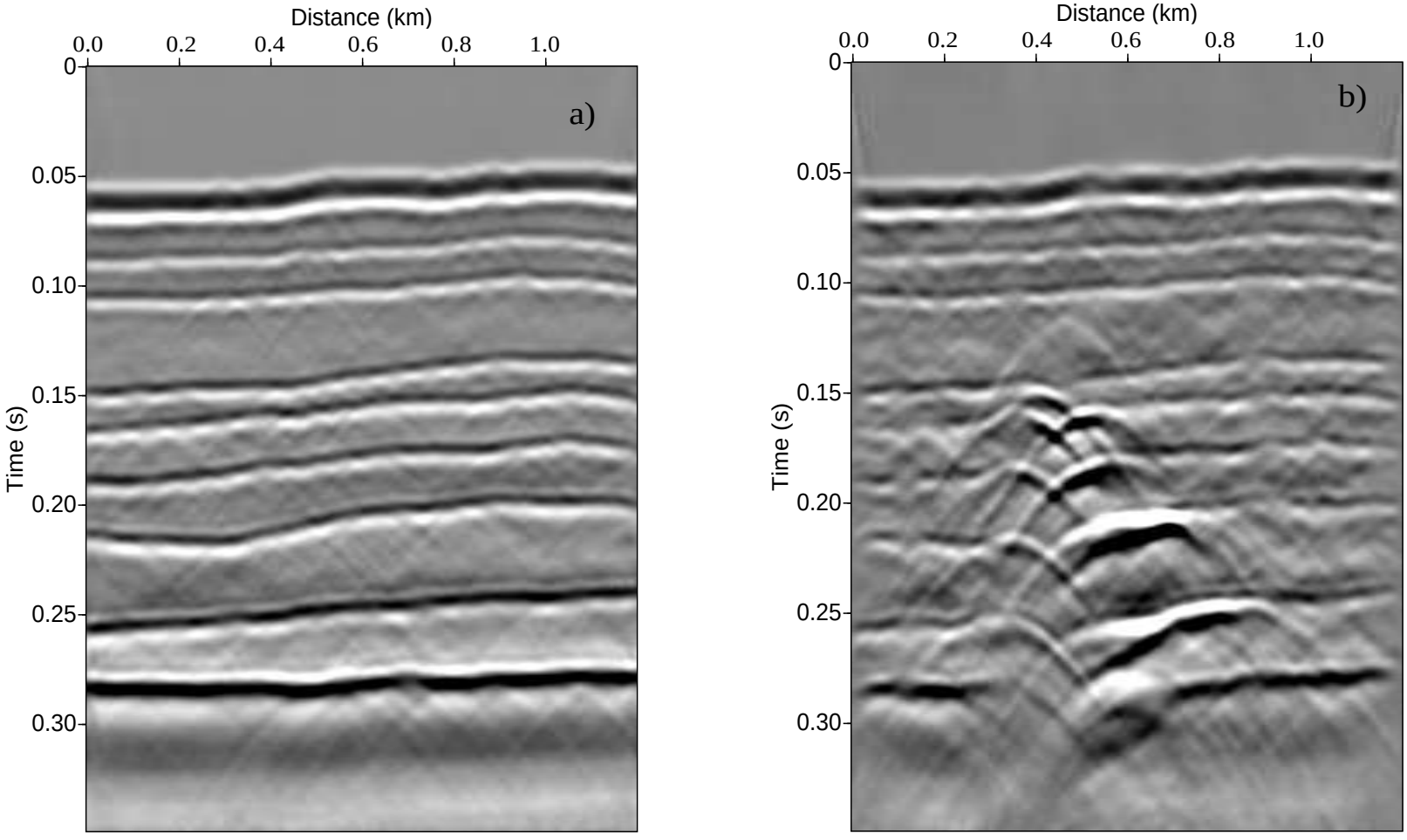

The preinjection seismogram (left) shows reflections from the mudstone layers. The reflections observed in the one-year seismogram (right) are due to the CO_2 accumulations below the deeper mudstone layers (see the one-year CO_2 saturation map).

Synthetic seismograms after 3 years (left) and 7 years (right) of CO_2 injection. The PUSHDOWN effect

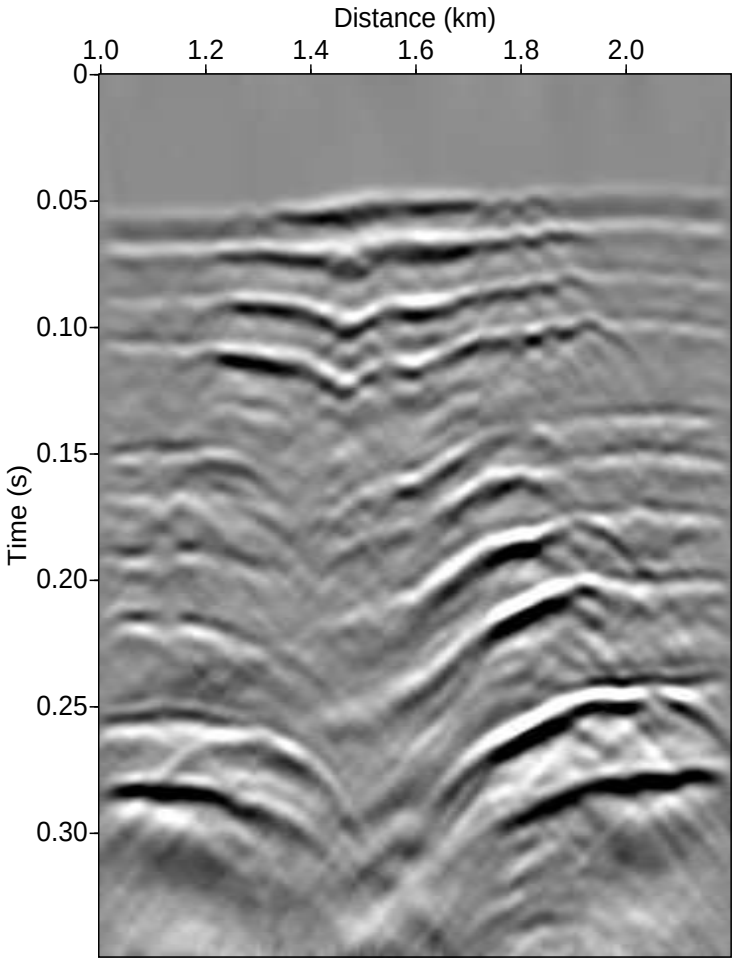

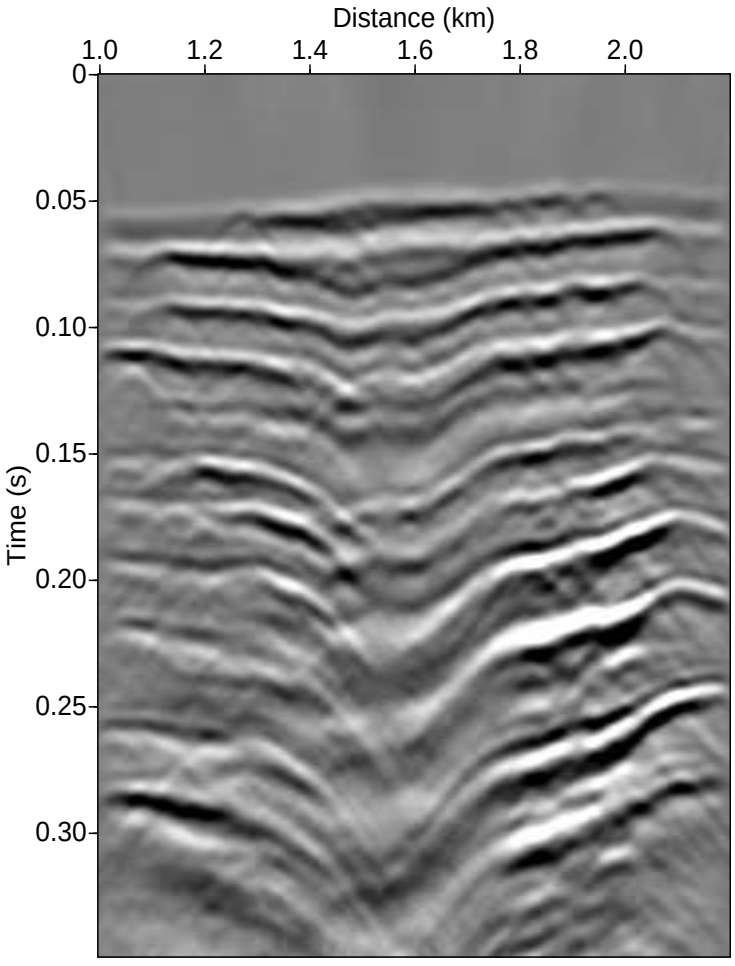

Note the delay and attenuation of the reflected waves in the center of the seismograms, more pronounced in the seven years one. These reflected waves travel in zones of low CO_2 accumulations. This time-lag is known as PUSHDOWN effect and is observed in real seismograms .

Synthetic seismograms after 3 years (left) and 7 years (right) of CO_2 injection. The PUSHDOWN effect

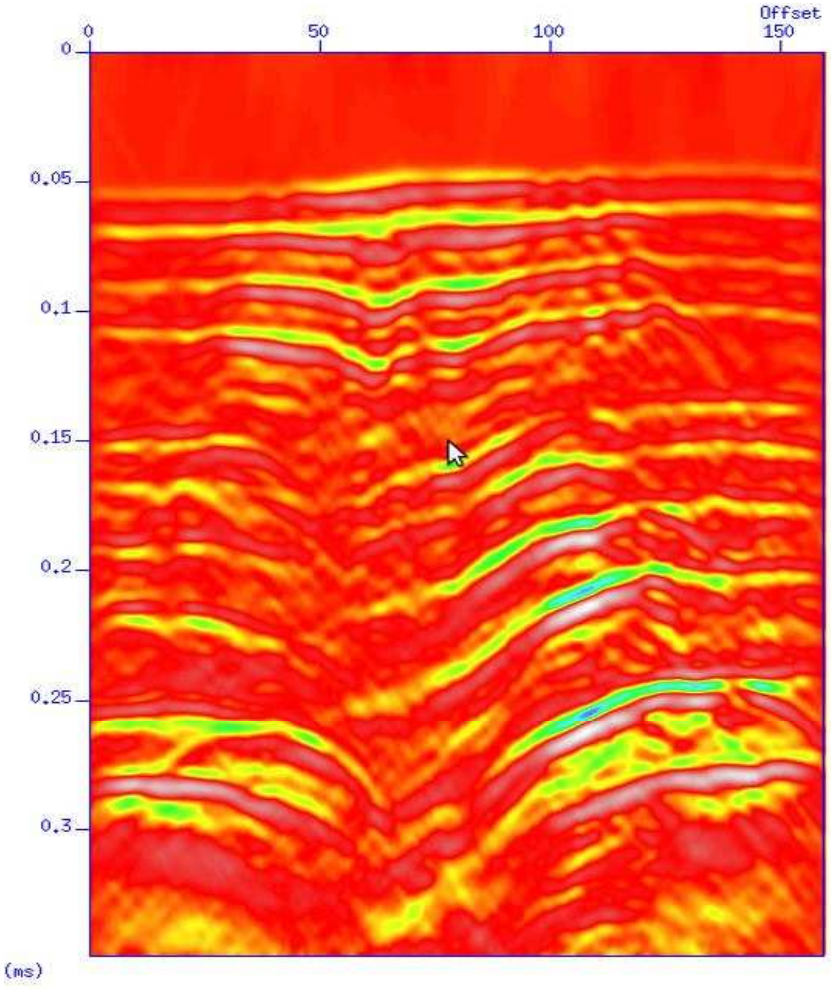

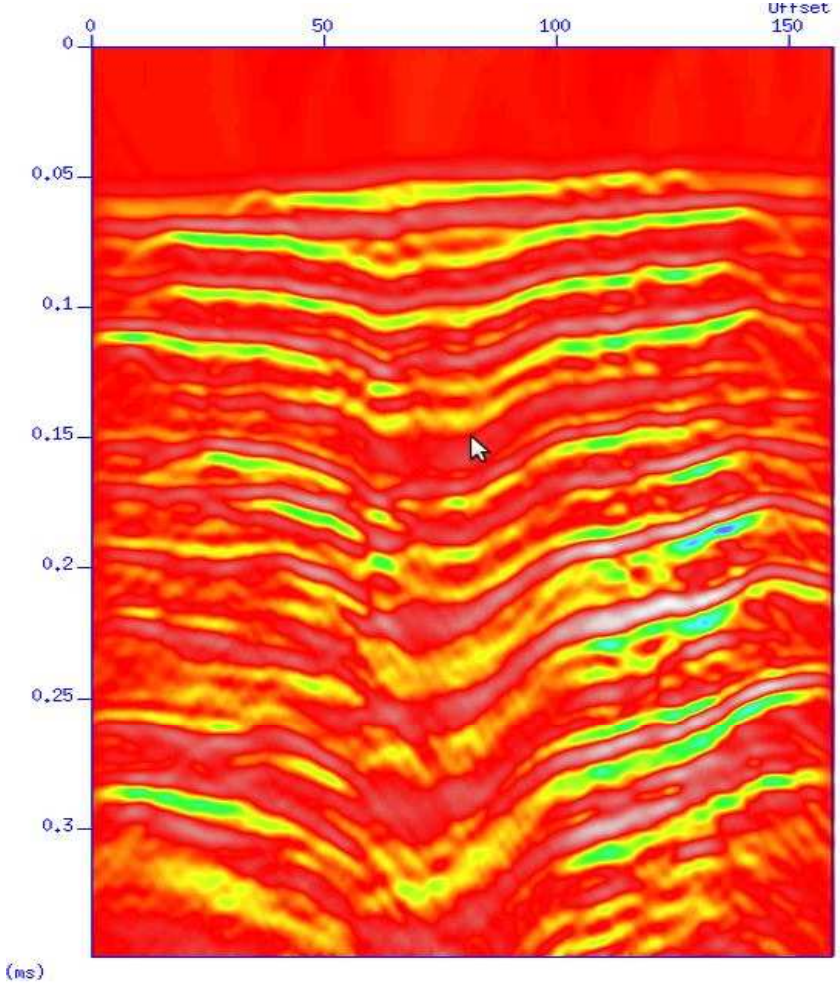

Note the delay and attenuation of the reflected waves in the center of the seismograms, more pronounced in the seven years one. These reflected waves travel in zones of low CO_2 accumulations. This time-lag is known as PUSHDOWN effect and is observed in real seismograms .

Real seismograms from the Sleipner field showing the PUSHDOWN effect.

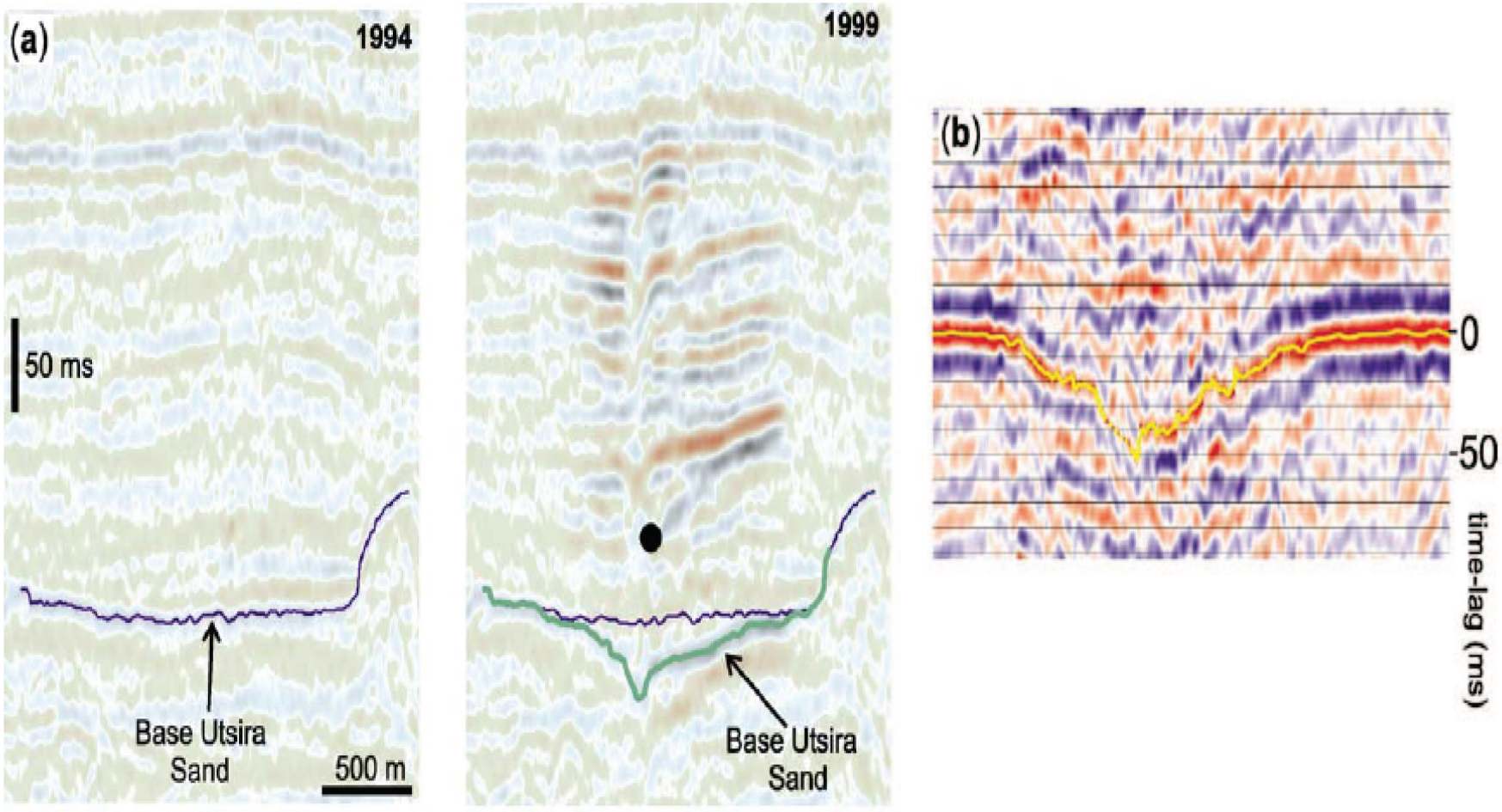

The synthetic seismograms display a similar 50 ms delay associated with the pushdown effect.

Influence of capillary pressure on the seismic response.

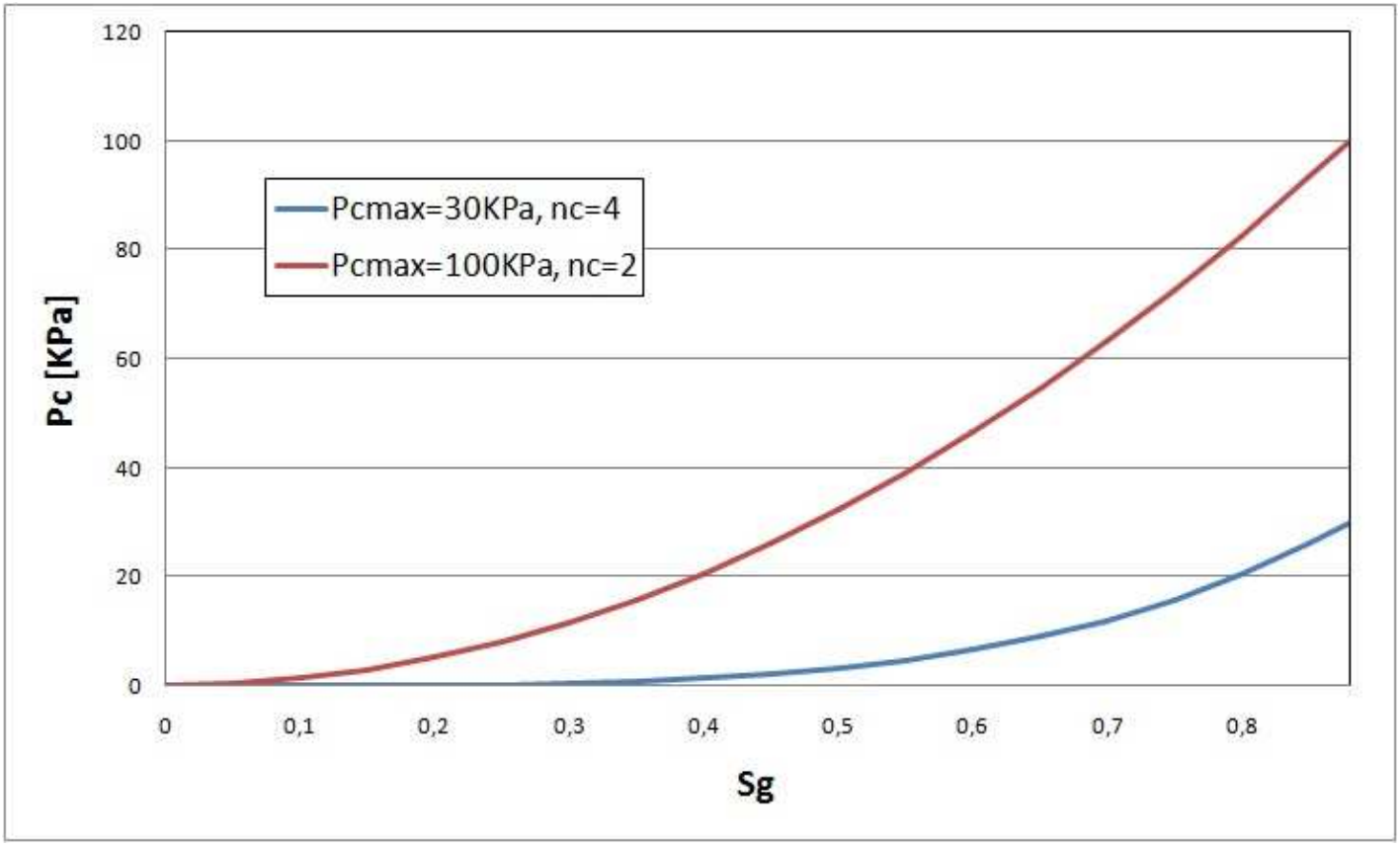

Left : Two different choices of the capillary pressure function used to simulate CO_2 injection. The choice Pcmax = 30 kPa, nc = 4 (blue curve) was used in the previous simulations.

Influence of capillary pressure on the seismic response. Seismograms after 3 years of injection

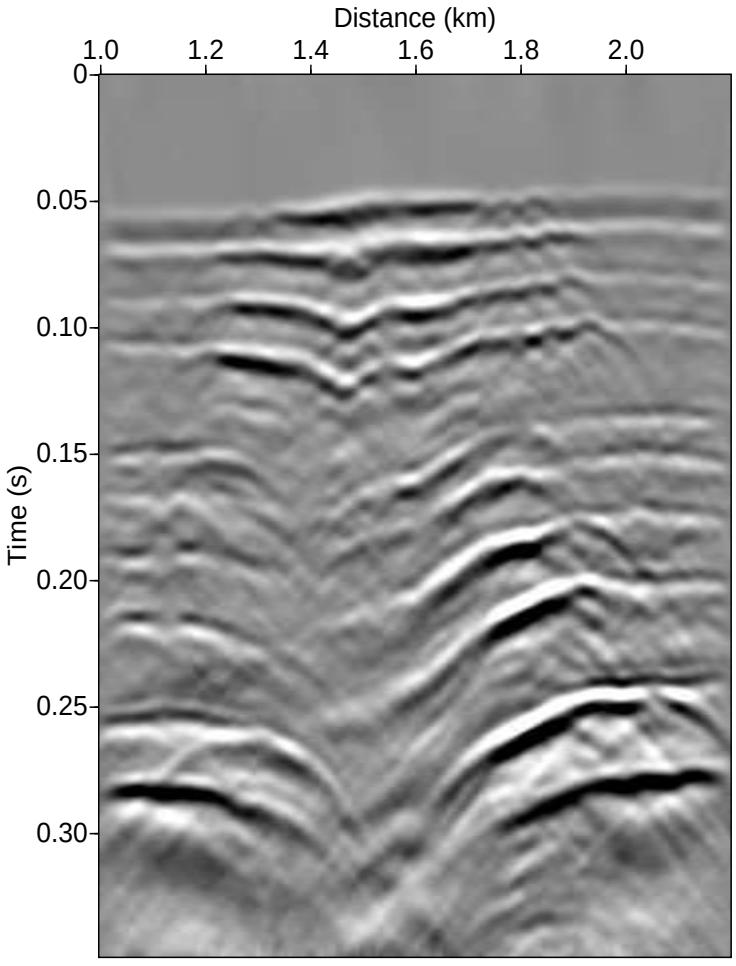

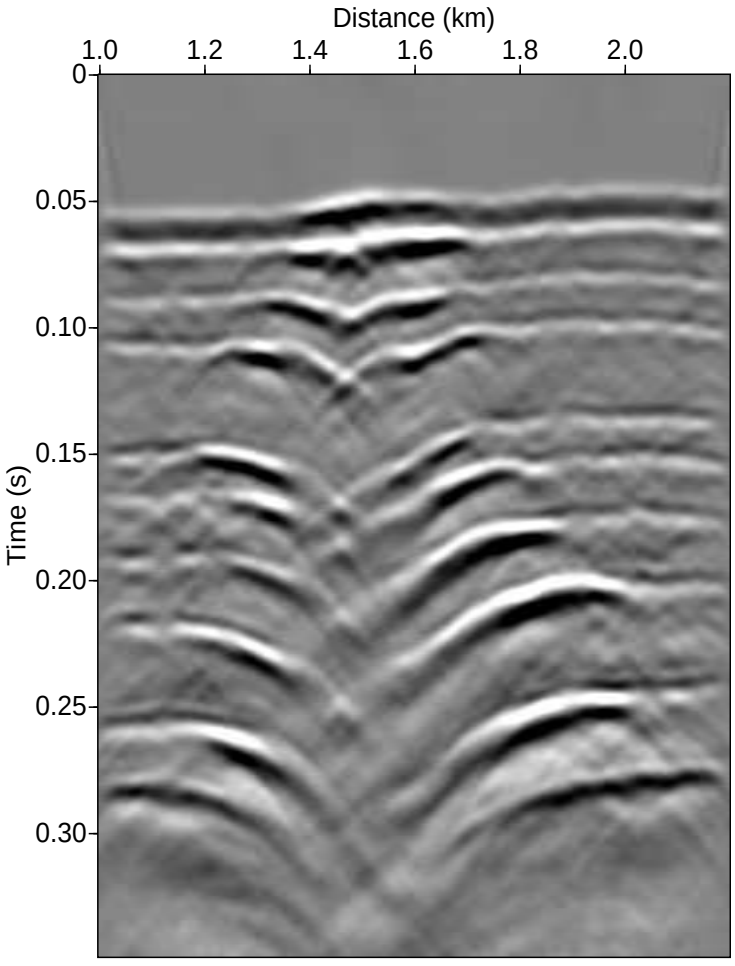

Left : Pcmax = 30 kPa, nc = 4. Right: Pcmax = 100 kPa, nc = 2.

Influence of capillary pressure on the seismic response. Seismograms after 7 years of injection

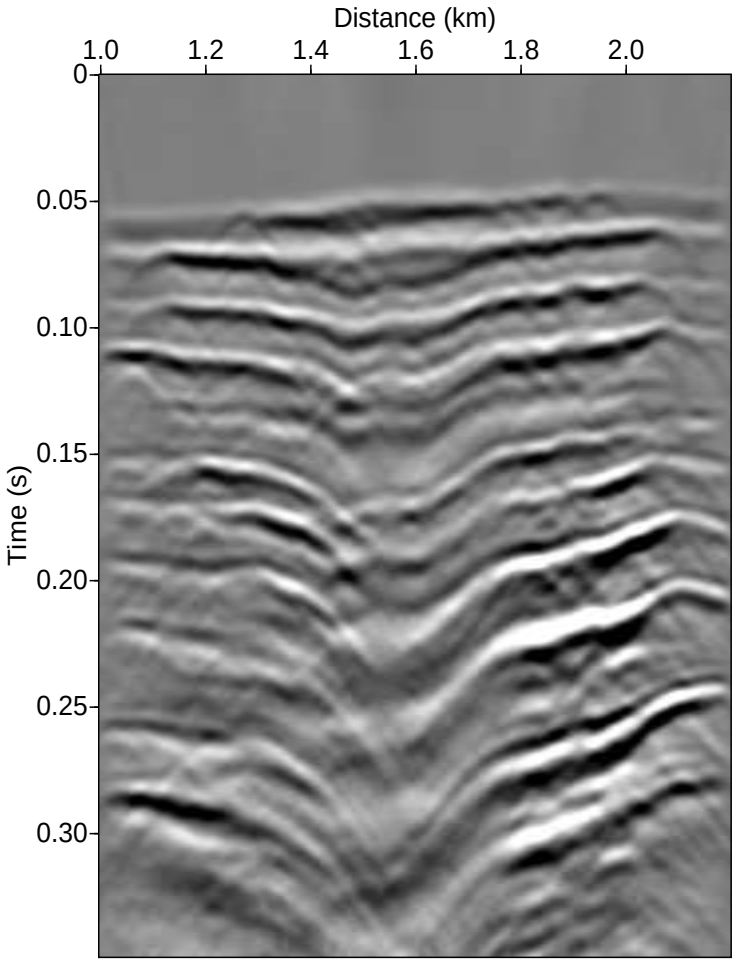

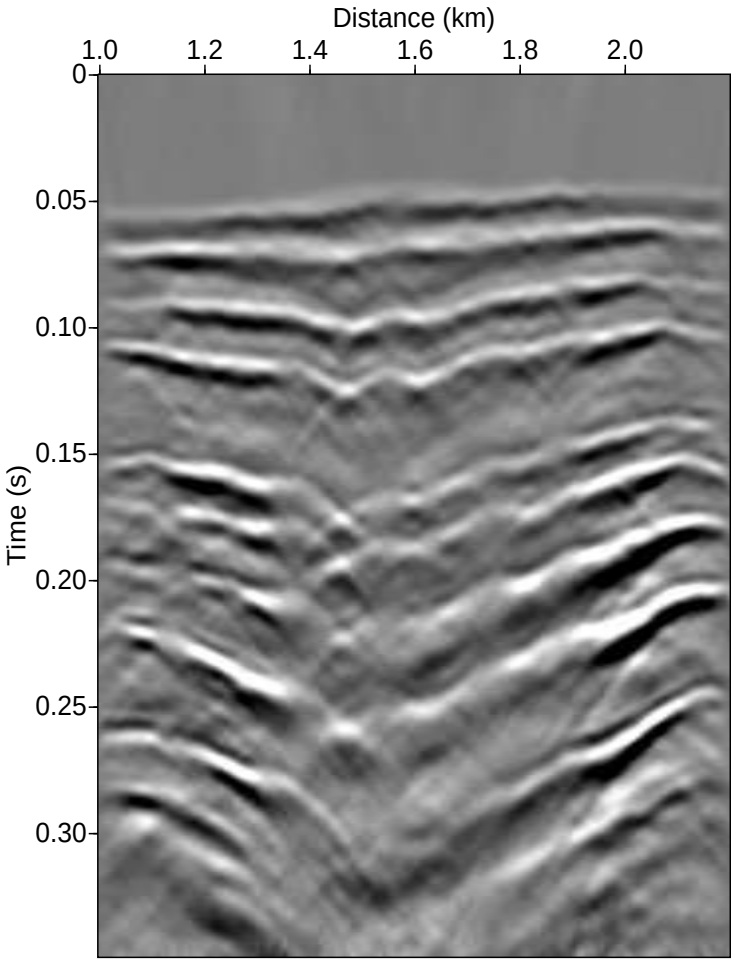

Left : Pcmax = 30 kPa, nc = 4. Right: Pcmax = 100 kPa, nc = 2.

CONCLUSIONS

- **The numerical examples show the effectiveness of combining multiphase flow simulators in porous media with seismic monitoring to map the spatio-temporal distribution of CO_2 after injection.**
- **The wave propagation model includes attenuation and dispersion effects due to mesoscopic scale heterogeneities using White's theory.**
- **This methodology constitutes a valuable tool to monitor the migration and dispersal of the CO_2 plume and to analyze storage integrity, providing early warning should any leakage occurs.**

AKNOWLEDGEMENTS

This work was partially funded by the European Union under project CO2 ReMoVe.

I wish to thank IMAL for allowing me to share this results.

THANKS FOR YOUR ATTENTION !!!!!!